Progress of Theoretical Physics, Vol. 70, No. 2, August 1983

Optical Model Potential in the Lowest Order Brueckner Theory and Complex Effective N-N Interaction

Norio YAMAGUCHI,*) Sinobu NAGATA* and Takaaki MATSUDA*

Nuclear Physics Laboratory, Oxford
**Department of Applied Physics, Faculty of Engineering*
Miyazaki University, Miyazaki 880

(Received March 26, 1983)

The optical model potential for a nucleon propagating inside the infinite nuclear medium is calculated in the Brueckner-Hartree-Fock approximation. It is found that the resultant optical potential, especially its imaginary part, strongly depends on the strength of the tensor component and the short-range behavior of the used realistic nuclear force. Our results for the real part show a large anomaly just above the Fermi momentum especially in lower density. This anomaly mainly comes from the $^3S_1+{}^3D_1$ state interaction. From the obtained transition matrix a complex effective N-N interaction with three-range-Gaussian form factor is constructed. This interaction reproduces the partial wave contributions to the optical potential in nuclear matter. By using the folding procedure, this effective interaction is applied to the $p+{}^{40}$Ca elastic scattering. The observed differential cross section and polarization are very well reproduced over a wide range of energies with only a renormalization of the imaginary potential strength.

§ 1. Introduction

The optical model potential (OMP) has been playing a remarkable role in describing the nuclear scattering phenomena and numerous refinements to it have been hitherto performed in order to fit the experimental data. Recently systematic and very accurate experimental data with polarized beams are presented and the detailed analyses of these data with OMP have been satisfactorily performed.[1)]

The microscopic theory of OMP has been developed in various ways[2)] and microscopic evaluations of it have been performed progressively in recent years.[3)~6)] Under those successes of fundamental confirmation of OMP, investigations of the nucleon-nucleus scattering based on the "realistic" nuclear force are now in their quantitative stage. One of the microscopic approach is what is called "nuclear matter approach". This approach has successfully explained the bulk properties of nuclei which appear in scattering problems such as the volume integral, root mean square radius, energy dependence of the real potential and the effective mass as well as fitting the experimental cross section. It is now widely recognized that the main part of OMP can be explained within the lowest order Brueckner theory (LOBT) starting from the realistic nuclear force.

In this paper, we intend to perform the following two-folds within the framework of LOBT in the nuclear matter approach.

(1) To estimate the reliability of the results by LOBT especially focussing on the dependence of the microscopic OMP on the realistic nuclear force.

Similar calculations have already been carried out by Brieva et al.[3)] (Oxford group) and by Mahaux et al.[4)] (Liege group). The latter group solved the scattering equation for an incident and a target nucleon in a rigorous way using the RHC potential[7)] and they obtained the OMP of finite nuclei $U_{\text{finite}}(r)$ from that of the infinite nuclear matter $U_\infty(r)$

*) On leave from the Faculty of Engineering, Miyazaki University, Miyazaki.

via the local density approximation (LDA) or an improved LDA. On the other hand, the Oxford group, starting from the HJ potential,[8] evaluated the density- and bombarding-energy-dependent complex effective N-N interaction ${}^{\text{eff}}t(r;\rho,E)$. This is advantageous for the application to a wide range of scattering aspects for finite nuclei. Their method of calculation, however, is an extended version of the reference spectrum method.[9] Considering the existence of some discrepancies[4] in results between Oxford group and Liege group, we are not certain whether these discrepancies are due to the different basic nuclear forces or due to the different calculational methods they use. Adding to the situation mentioned above, just as it has been the case for the bound state problem,[10] it is probable that the lowest order results may fairly be changed by incorporating correlation diagrams and rearrangement diagrams. Hence, before proceeding to the higher order calculation, it is necessary to clarify to what extent the lowest order results will be reliable and be affected, even in the same method, by basic nuclear forces. This is the first purpose of this paper.

(2) Evaluation of the complex effective N-N interaction in the analytic form.

There are some prescriptions to apply the results for nuclear matter to finite nuclear systems. The use of LDA for one-body potential is one of them. Because of the short range of the interaction, it is likely that LDA works well in the region where the density varies gradually. In the surface region, however, finite range effects of the interaction should be taken into account.[4] The foldng method of an effective interaction can take into account this effect naturally. It is very difficult, however, to express the density and energy dependences of the effective interaction ${}^{\text{eff}}t(r;\rho,E)$ in the analytic form and the Oxford group used the effective interaction only numerically, thus with the restricted applications. On the other hand, "semi-realistic" effective interactions such as M3Y[11] or G3Y[12] have been successfully applied for the calculation of the folding potential of nucleon- and nucleus-nucleus scattering.[13] So it is highly desired to evaluate a microscopically confirmed effective interaction with some analytic form in the sense that it will give some criterions for "semi-realistic" interactions in model calculations. Hence, our second purpose of this paper is to derive a new density- and bombarding-energy-dependent complex effective N-N interaction with an analytic form on the basis of the microscopic calculation for the scattering system.

In § 2 our formulation and procedure are shown. The results and discussion are given in § 3. In this section we discuss the obtained OMP especially focussing on its density- and energy dependences relating to the difference of the realistic nuclear forces and on the anomaly of the real potential just above the Fermi momentum. We also argue on the applicability of our complex effective N-N interaction to the $p+{}^{40}$Ca elastic scattering. In § 4 a summary is given.

§ 2. Formulation

2.a. *Brueckner-Hartree-Fock approximation*

It has been shown by Bell and Squires[2] that OMP can be identified with the mass operator of the one-body Green's function for a nucleon propagating through nuclear medium. In the case of nuclear matter, the Green's function is expressed in the momentum representation as follows:

$$G(k, E)=\left(E-\frac{\hbar^2}{2m}k^2-M(k, E)\right)^{-1}, \tag{2·1}$$

where $M(k, E)$ is the complex mass operator,

$$M(k, E)=V(k, E)+iW(k, E). \tag{2·2}$$

The energy E and momentum k of the propagating nucleon are related by the dispersion equation,

$$E=\frac{\hbar^2}{2m}k^2+M(k, E). \tag{2·3}$$

Assuming that the imaginary part is small, the phenomenological OMP is derived in the first order approximation as follows:[4]

$$\text{Real OMP}=\text{Re}\, M(k,\epsilon(k))=V(k, \epsilon(k)), \tag{2·4}$$

$$\text{Imaginary OMP}=\left(\frac{m_E}{m}\right)^{-1}\cdot \text{Im}\, M(k, \epsilon(k))=\left(\frac{m_E}{m}\right)^{-1}\cdot W(k,\epsilon(k)), \tag{2·5}$$

where m_E/m is the energy mass defined by

$$\frac{m_E}{m}=\left(1-\frac{\partial\, \text{Re}\, M(k, E)}{\partial E}\right)_{E=\epsilon(k)}, \tag{2·6}$$

and $\epsilon(k)$ is now a real energy given by

$$\epsilon(k)=\frac{\hbar^2}{2m}k^2+\text{Re}\, M(k, \epsilon(k)). \tag{2·7}$$

We expand the mass operator in nuclear matter in terms of the density similar to the hole-line expansion[14] of the Brueckner-Bethe theory for the binding problem. The convergence of this expansion is assured by the small parameter (wound integral) $\varkappa$ (~ 0.15).[15] Graphical representations of some leading terms are shown in Fig. 1. The Brueckner-Hartree-Fock (BHF) approximation, we adopt here, incorporates only the lowest order diagram (a) and the mass operator can be expressed as

$$U_\infty(E(k); k_F)=V_\infty(E(k); k_F)+iW_\infty(E(k); k_F)=\sum_{|\boldsymbol{k}_j|<k_F}\langle \boldsymbol{k}\boldsymbol{k}_j|t(E+\varepsilon(k_j))|\boldsymbol{k}\boldsymbol{k}_j\rangle_A, \tag{2·8}$$

where the operator t is the transition matrix in nuclear medium or the complex reaction matrix and is the solution of the following two-nucleon scattering equation:

$$\langle \boldsymbol{k}\boldsymbol{k}_j|t(\omega)|\boldsymbol{k}\boldsymbol{k}_j\rangle=\langle \boldsymbol{k}\boldsymbol{k}_j|v|\boldsymbol{k}\boldsymbol{k}_j\rangle+\sum_{|\boldsymbol{k}_a|,|\boldsymbol{k}_b|>k_F}\frac{\langle \boldsymbol{k}\boldsymbol{k}_j|v|\boldsymbol{k}_a\boldsymbol{k}_b\rangle\langle \boldsymbol{k}_a\boldsymbol{k}_b|t(\omega)|\boldsymbol{k}\boldsymbol{k}_j\rangle}{\omega-e(k_a)-e(k_b)+i\delta}. \tag{2·9}$$

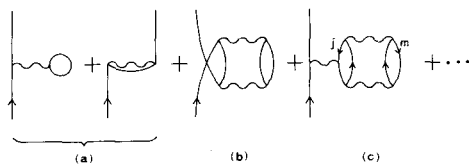

Fig. 1. Some leading terms in the perturbation expansion for the optical potential. The wavy lines represent the renormalized interactions of the ladder correlation.

Hereafter E is real and satisfies Eq. (2·7).

In Eq. (2·9), v is a basic nuclear force and $e(k)$ is the energy spectrum of intermediate states. The potential energy for intermediate states, generally, should be calculated with including the property of off-energy-shell propagation. But we use the same definition as Eq. (2·7) for simplicity. It is also noted that the energy $\varepsilon(k_j)$ in Eq. (2·8) is that of a single particle bound state in the target nucleus. Thus this energy is usually calculated with the so-called QTQ spectra for intermediate states. But we also use the same definition as the particle state energy Eq. (2·7) for simplicity. The latter approximation does not seem so unrealistic, considering the situation that the two-body nuclear force usually gives less attractive binding energy and the use of Eq. (2·7) for the spectra gives rise to deeper single particle energies.

Diagram (b) is the Pauli-rearrangement diagram and it is not so easy to calculate this contribution exactly because it is necessary to take into account the contributions from high intermediate states. Diagram (c) is the starting-energy (ω-) rearrangement diagram and is expressed as

$$(\mathrm{c}) = -\bar{\chi}\sum_{\boldsymbol{k}_j}\langle \boldsymbol{k}\boldsymbol{k}_j|t|\boldsymbol{k}\boldsymbol{k}_j\rangle_A\,, \tag{2·10}$$

where $\bar{\chi}$ represents the wound integral, Eq. (2·11), averaged over $\boldsymbol{k}_j$ for each k_F:

$$\chi_j = \sum_{\boldsymbol{k}_m}\langle \boldsymbol{k}_j\boldsymbol{k}_m|\frac{g}{\mathcal{E}}\frac{g}{\mathcal{E}}|\boldsymbol{k}_j\boldsymbol{k}_m\rangle_A \tag{2·11}$$

with g being the reaction matrix in the target nucleus and $\mathcal{E}^{-1}$ the propagator. With this approximation we obtain the OMP renormalized with the ω-rearrangement diagram as

$$U_\omega(E(k);\, k_\mathrm{F}) = (1-\bar{\chi})\sum_{\boldsymbol{k}_j}\langle \boldsymbol{k}\boldsymbol{k}_j|t|\boldsymbol{k}\boldsymbol{k}_j\rangle_A\,. \tag{2·12}$$

In this paper, we first calculate the self-consistent Eqs. (2·7)~(2·9) and secondly we discuss the contribution of diagram (c) by using Eq. (2·12) for the OMP. In the second case we do not perform a self-consistent calculation with Eq. (2·12).

2.b. *Computational procedures*

We extend the computational procedure of BHF calculation in the bound state problem of nuclear matter[16] to the scattering problem. It is rather straightforward but there are some points to be taken care of for the accurate calculation. The first point is how to deal with the pole in the Green's function and the complex quantities. We follow the methods used in Ref. 4). The second point is an approximation to the particle state spectrum by suitable analytic functions since it shows an anomaly just above the Fermi momentum.

For a given Fermi momentum k_F and incident momentum k, we first solve the following equation to obtain the relative scattering wave function u for each two-nucleon eigenstate,

$$u_{ll'}^{IST}(r;\, q) = S_l(r;\, q)\delta_{ll'} + 4\pi\sum_{l''}\int r'^2 dr'\, F_l(r,\, r';\, q)\mathcal{V}_{l'l''}^{IST}(r')u_{ll''}^{IST}(r';q)\,. \tag{2·13}$$

The notations in the above equation are the same as those in Ref. 17). In solving the

above equation, we use the angle-averaged Pauli function and center-of-mass momentum $\bar{P}$ for a given k and relative momentum q. It is checked that this approximation scarcely affect the results. Once the wave function is obtained, we can calculate the transition matrix element and the one-body potential by the following equations:

$$\langle q|t_{ll}^{JST}|q\rangle=-\frac{j_l^2(qr_c)}{G_l(r_c, r_c)}+4\pi\sum_{l'}\int_{r_c}r^2drS_l(r; q)\mathcal{V}_{ll'}^{JST}(r)u_{ll'}^{JST}(r; q) \tag{2·14}$$

and

$$U_\infty(E(k); k_F)=\frac{1}{2\pi^2}\int q^2dqZ(q; k, k_F)\sum_{JSTl}(2J+1)\frac{(2T+1)}{2}\langle q|t_{ll}^{JST}|q\rangle, \tag{2·15}$$

where

$$Z(q; k, k_F)=\frac{1}{kq}(k_F^2-(k-2q)^2). \tag{2·16}$$

To obtain the single particle spectrum for higher intermediate momenta, we represent the real part of the one-body potential Eq. (2·15) by quadratic polynomials for k smaller than 1.8 k_F and in the Woods-Saxon form for k larger than 1.6 k_F. In this fitting procedure, we skip the momenta around which an anomaly of the real potential occurs.

2.c. *Complex effective N-N interaction*

The transition matrix in nuclear matter or the complex reaction matrix Eq. (2·9) is considered to be an effective interaction between the incoming nucleon and a target nucleon because it renormalizes high-momentum-ladder correlations in nuclear medium. It is a non-local and complex operator and depends on the starting energy ω and Fermi momentum k_F. In order to apply it to the problems of finite nuclei, it is desired to obtain an averaged local effective interaction in the coordinate space. Leaving k_F and $E(k)$ as fixed parameters, we average over q (and P) so as to reproduce the BHF potential for the incident particle when used in the Born approximation. Such average is given as follows:

$${}^{\text{eff}}t_{ll'}^{JST}(r; k_F, E(k))=\frac{\int q^2dqZ(q; k, k_F)j_{l'}(qr)\sum_{l''}\mathcal{V}_{ll''}^{JST}(r)u_{ll''}^{JST}(r; q)}{\int q^2dqZ(q; k, k_F)j_{l'}(qr)j_l(qr)}. \tag{2·17}$$

We decompose the obtained effective interaction to the central and non-central components respectively using the multipole expansion.[18]

Once the effective interaction is obtained in the coordinate space, we try to parametrize it by a linear combination of Gaussian form factors with three (two for LS) ranges at each k_F and E. The k_F- and E-dependences are neglected for the non-central components, because they are considered to be not so important. Their strengths are determined to fit the numerical results at $k_F=1.1$ fm^{-1} and $E=48.6$ MeV.

$$\begin{aligned}&{}^{\text{eff}}t^{ST}(r; k_F, E)=\sum_i v_i^{ST}(k_F, E)e^{-(r/\lambda_i)^2}; \quad \text{central and LS},\\ &{}^{\text{eff}}t^{ST}(r)=\sum_i v_{0i}^{ST}r^2e^{-(r/\lambda_i)^2} \quad ; \quad \text{tensor}.\end{aligned} \tag{2·18}$$

The dependence of the parameter $v_i(k_F, E)$ on k_F and E is rather smooth but not so simple to be expressed as a separable form. For most calculations with the effective interaction, the bombarding energy is fixed and so we only simulate the k_F dependence by the following

function for the fixed energy:

$$v_i(k_F, E)=v_{0i}(E)(1+\alpha_i(E)k_F+\beta_i(E)k_F{}^2). \tag{2·19}$$

In order to check the applicability of the present functionalized complex effective interaction, we calculate the folding potential for the elastic scattering of proton from ^{40}Ca with the local momentum approximation as follows:[3]

$$U_F(\boldsymbol{r}_1; E)=\int\rho(\boldsymbol{r}_2)T_D(\boldsymbol{r}_1, \boldsymbol{r}_2; k_F, E)d\boldsymbol{r}_2+\int\rho(\boldsymbol{r}_1, \boldsymbol{r}_1')T_{EX}(\boldsymbol{r}_1, \boldsymbol{r}_1'; k_F, E)j_0(k|\boldsymbol{r}_1-\boldsymbol{r}_1'|)d\boldsymbol{r}_1', \tag{2·20}$$

where

$$k=\left(\frac{2m}{\hbar^2}(E-\mathrm{Re}\ U_F(\boldsymbol{r}_1; E))\right)^{1/2} \tag{2·21}$$

$$T_{D,EX}=\frac{1}{16}(\pm t^{00}+3t^{10}+3t^{01}\pm 9t^{11}), \tag{2·22}$$

and $\rho(\boldsymbol{r}, \boldsymbol{r}')$ is approximated as[19]

$$\rho(\boldsymbol{r}, \boldsymbol{r}')=\rho\left(\frac{\boldsymbol{r}+\boldsymbol{r}'}{2}\right)\frac{3}{(sk_F)^3}(\sin(sk_F)-(sk_F)\cos(sk_F)) \tag{2·23}$$

with $s=|\boldsymbol{r}-\boldsymbol{r}'|$ and taking k_F in the effective interaction as $\rho=\rho((\boldsymbol{r}_1+\boldsymbol{r}_2)/2)$ $=(2/(3\pi^2))k_F{}^3$. In comparing with phenomenological OMP, the localized imaginary potential in Eq. (2·20) should be multiplied by the effective k-mass according to the consideration of the mean free path :[20]

$$\text{Im. of the phenomenological OMP} \Leftrightarrow \frac{m_k}{m}W_F=\left(1+\frac{m}{k}\frac{\partial V_\infty}{\partial k}\right)^{-1}\cdot W_F, \tag{2·24}$$

where W_F is the imaginary part of U_F in Eq. (2·20)

§ 3. Results and discussion

We calculate the transition matrix elements and the optical potential $U_\infty(E(k); k_F)$ at four Fermi momenta, $k_F=1.4$, 1.1, 0.8 and 0.5 fm^{-1}, taking into account the partial waves $J\leqq 3$.

3.a. *Characteristics of OMP in nuclear matter*

We use two different "basic" nuclear forces. One of them is the HJ potential and the other is OPEG potential.[21] HJ has a typical hard core and OPEG is a soft core one. Hence, we can discuss the effect of the different character of nuclear forces on the resultant OMP. It is well known that HJ brings about 8 MeV/A of the binding energy of nuclear matter and OPEG gives 11 MeV/A. This situation will hold in the scattering problem at lower incident energies and near the normal density.

3.a.1. *Real part of OMP*

We first show the incident momentum ($k-$) dependence of $V_\infty(E(k); k_F)$ at each k_F in Fig.2(a) and some partial wave contributions to it in Fig. 2(b). It is clearly seen from Fig. 2(a) that the results by OPEG and HJ are largely different from each other especially in

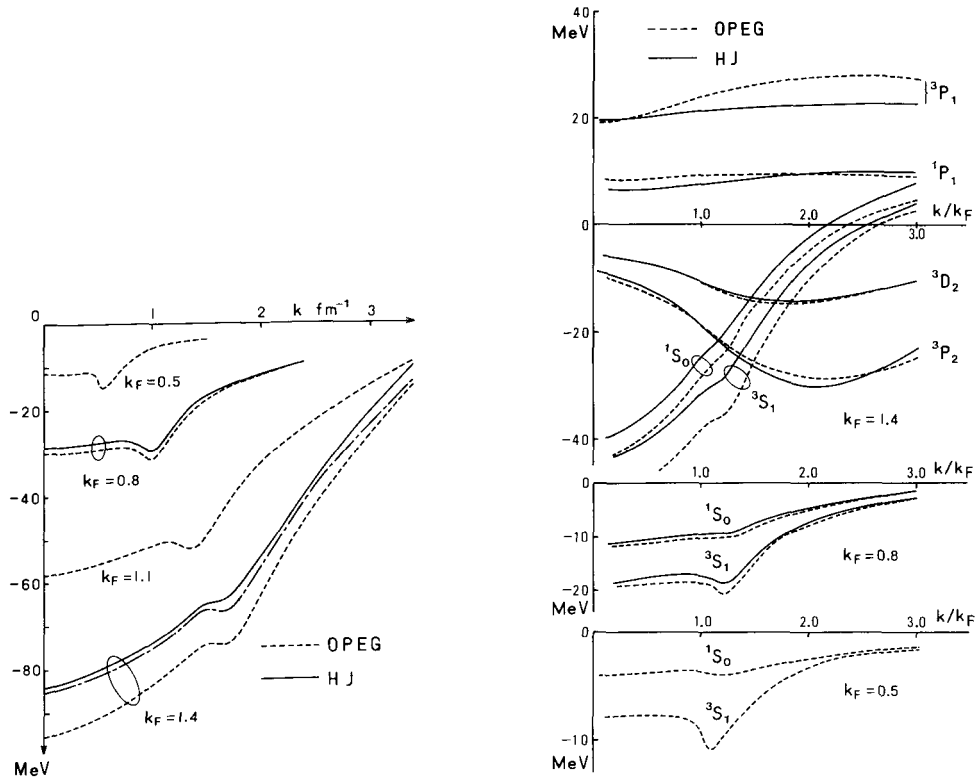

Fig. 2.(a) The incident momentum k dependence of the real part of OMP $V_\infty(E(k); k_F)$ at $k_F=0.5$, 0.8, 1.1 and 1.4 fm^{-1}. The dash-dotted line denotes $(1-\bar{x})V_\infty(\mathrm{OPEG})$ at $k_F=1.4$ fm^{-1}.
(b) Some partial wave contributions to $V_\infty(E(k); k_F)$.

high density and low energy regions. We find that the nearly constant differences hold in the energy region of the bound states and Fig. 2(b) shows that the $^3S_1$ and $^1S_0$ states are responsible for these differences. The reason why such differences arise should be attributed to the Pauli effect on the ladder correlation generated by the nuclear forces with different core nature and different ^3E tensor strength relative to the central part. It is well known that the ratio of the tensor to central parts of the nuclear force is essential to the result of the binding energy.[16] Then we can see in Fig. 2 that these discrepancies are reduced as k_F is decreased where the Pauli projection is less effective.

For a comparison with phenomenological OMP we parametrize the E-dependence of our $V_\infty(E; k_F)$ in the linear approximation and obtain

$$\left.\begin{aligned} V_\infty(E; k_F=1.4, \mathrm{OPEG}) &= -(71.1-0.36E) \\ V_\infty(E; k_F=1.4, \quad \mathrm{HJ}) &= -(63.6-0.31E) \end{aligned}\right\} \quad \text{for } E \lesssim 50 \text{ MeV}. \tag{3·1}$$

We find that the depth and energy-dependence are very large for the OPEG case comparing with $V=-(56.5-0.3E)$[4] obtained from RHC potential which has a large hard-core range and large tensor to central ratio. We may say that the real part of the microscopic OMP depends rather strongly upon the basic nuclear force from which it is calculated.

Here we discuss the effect of the ω-rearrangement correction in the approximation of Eq. (2·12), in which we use $\bar{x}$ for each k_F extracted from our previous bound state

calculation[22] and parametrized as

$$\bar{x} = 0.04184\, k_F \cdot (1 + 0.5920\, k_F). \tag{3·2}$$

In Fig. 2(a) a result is plotted for the OPEG case. Accidentally it is almost equal to that by the HJ potential without the renormalization and can be expressed as

$$(1-\bar{x}) \cdot V_\infty(E; k_F = 1.4, \text{OPEG}) = -(63.5 - 0.32E) \qquad \text{for } E \lesssim 50 \text{ MeV}. \tag{3·3}$$

Of course the values of $\bar{x}$ are larger for hard-core potentials, then the depths in the case of HJ and RHC will further be reduced by more than 10% near the normal density.

3.a.2. *Anomaly in real OMP*

Our results show a significant anomaly in $V_\infty(E; k_F)$ just above the Fermi momentum as is seen in Fig. 2(a). This plateau is related to the enhancement of the effective mass near the Fermi surface and detailed discussion on this anomaly has been given in Refs. 4) and 23). It has not been shown explicitly, however, that only the ladder correlation, Fig. 1(a), can yield this anomaly when we start from the realistic nuclear forces.

Here we point out that this plateau can be explained in terms of the revival of the Pauli-excluded momentum space and of the strong low-momentum-components of the interaction in the $^3S_1$ state. First it is noticed that this anomaly is predominantly from the $^3S_1$ partial wave as seen in Fig. 2(b). Matrix elements of t are affected by the propagation in the intermediate state, that is, by the Pauli rejection, transition matrix elements to the intermediate states and the energy denominator. In the bound state problem, momenta of the two interacting nucleons are both below k_F and so the Pauli

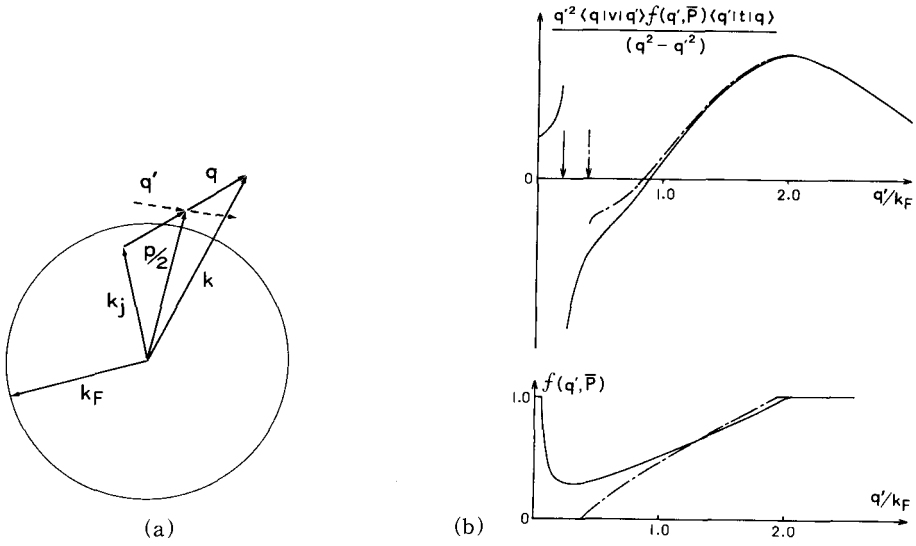

Fig. 3.(a) Schematic picture of relevant momenta in the case of an incident momentum k just above k_F. k_j is a target-nucleon-momentum, q is a starting relative momentum and q' is an intermediate one, which is not prohibited by the Pauli exclusion. P is the total momentum.

(b) Illustrative figure for the revival of Pauli-excluded momentum space. The lower part shows the Pauli functions $f(q', \bar{P})$ of $k = 1.2\, k_F$ for $q = 0.2\, k_F$ (solid line) and $0.4\, k_F$ (dash-dotted line). In the upper part an illustration for the q'-dependence of the integrand in the second term of Eq. (2·9) in the case of the $^3S_1$ state. The ordinate is in an arbitrary unit. Arrows point to the positions of the pole.

function falls to zero in any case as the intermediate relative momentum q' decreases. In the scattering problem, however, an incident momentum k is beyond k_F and there are possibilities that these small q' is not prohibited. We illustrate such a case in Fig. 3(a) and the lower part of Fig. 3(b). In a case where k is a little beyond k_F, say, 1.2 k_F, small starting momenta q are included and the transition matrix elements to the intermediate states with "revived" small q', $\langle q'|t|q\rangle$, are very large especially in the ${}^3S_1+{}^3D_1$ state because of the tensor coupling. In an example of the soft core potential, $\langle q|v|q'\rangle$ is negative for such small q and q' and so the integration over q' in this Pauli-revived region in the last term of Eq. (2·9) gives an additional attractive contribution. The situation is schematically illustrated in the upper part of Fig. 3(b).

For a high k the starting momenta q also become large and so the position of the pole moves to the intermediate region of the Pauli-revived momenta. Thus the attractive contribution is cancelled. As k_F decreases, the relevant q and q' become very small and so their matrix elements are more attractive. Thus the resulting anomaly becomes more pronounced. The above interpretation is confirmed by taking the Pauli function with smooth cutoff for small q', which leads to the disappearance of the anomaly.

A similar result of the anomaly in the real potential is also reported recently by Haider et al.[24]

3.a.3. *Imaginary part of OMP*

The k- and k_F-dependences of the imaginary part $W_\infty(E(k); k_F)$ and some partial wave contributions to it are shown in Figs. 4(a) and (b), respectively. From these figures we notice that the imaginary part of OMP has a steep increment just above the Fermi energy and that this is mostly attributed to the ${}^3S_1$ state contribution. This steep increment is directly related to the plateau in the real potential through the dispersion relation.[23] We again notice that the imaginary part $W_\infty(E(k); k_F)$ is more strongly dependent on basic nuclear forces than the real potential. At $k_F=1.4$ fm^{-1} and $E=10$ MeV, the difference

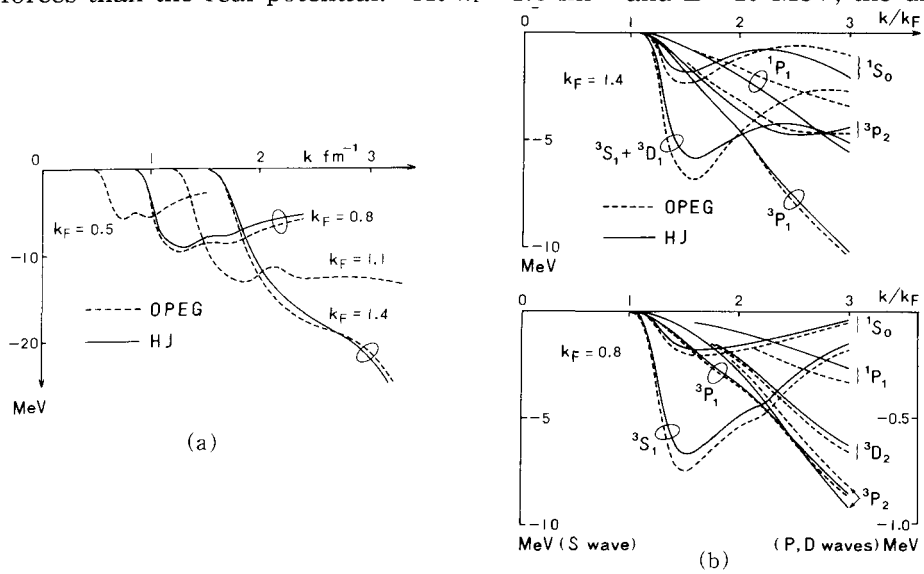

Fig. 4.(a) The incident momentum k dependence of the imaginary part of OMP $W_\infty(E(k);k_F)$ at $k=0.5$, 0.8, 1.1 and 1.4 fm^{-1}.
(b) Some partial wave contributions to $W_\infty(E(k); k_F)$.

between the OPEG and HJ results amounts to ~30%. As is evident in the expression of W_∞,[4]

$$W_\infty(E(k); k_F) = -\sum_{j,a,b} \pi n_<(j) n_>(a) n_>(b) |\langle \boldsymbol{kj}|t|\boldsymbol{ab}\rangle|^2 \delta(E+\varepsilon_j - e_a - e_b). \qquad (3\cdot4)$$

The imaginary part is governed by the strength of the interaction and the energy-conserved level density under the Pauli exclusion effect. The present difference is due to the character of the basic nuclear force connected with the mechanism discussed above for the different results of the real part and the occurrence of the anomaly. Thus we can conclude that the magnitude of the microscopic $U_\infty(E(k); k_F)$, especially $W_\infty(E(k); k_F)$, strongly depends upon the character of the basic nuclear force.

It is seen in Fig. 4(a) that W_∞ shows a wavy behavior. This comes from the fact that E-dependences of the S-wave-contributions to W_∞ quite differ from those of higher partial waves as seen in Fig. 4(b). For S waves, the transition matrix elements in Eq. (3·4) go near zero at the energy about $E=200$ MeV because of the repulsive core. On the contrary, higher-partial-wave contributions increase monotonically as the energy increases. As a consequence of the superposition of these different tendencies $W_\infty(E(k); k_F)$ has a wavy structure (except very small k_F, for example, $k_F=0.5$ fm^{-1}).

3.b. *Complex effective N-N interaction*

3.b.1. *Numerical results of* ${}^{eff}t(r; k_F, E)$

In the present calculation, the correlated wave function $u(r; q)$ generally causes a phase shift and does not heal to the unperturbed one. Then the effective interaction obtained through Eq. (2·17) will contain these shifts though in an averaged way. Thus it is expected that the behavior of the tail of the interaction will vary according to k_F and E. We show this example in Fig. 5 where the basic OPEP tail is also plotted for the real part for comparison. We find that the even components show a rather strong E-dependence at lower k_F. Hence we may say that the density and energy independent OPEP tail will not be accurate enough for the even-state effective interaction. On the contrary, the odd components almost heal to the bare one for the energy region $E \lesssim 150$ MeV.

As for the imaginary part, as is supposed from the behavior of the imaginary potential W_∞ in Fig. 4, the effective interaction, especially its even components, also has strong and complicated k_F- and E-dependences as a reflection of the Pauli effect and the coupling with the real part. One remarkable characteristics of the imaginary central components is that the triplet even component is, as seen in Fig. 5(c), drastically argumented as k_F decreases. This will guarantee the steep increment of W_∞.

We show the radial behavior of the non-central components in Figs. 6(a) and (b) where the functionalized effective interaction (CEG in the next subsection) and the basic OPEG potential are also plotted. It is found that the real parts are rather similar to the original non-central forces respectively. On the contrary, the imaginary non-central components have quite different radial dependences from those of the real parts and are strongly dependent on k_F and E.

3.b.2. *Complex effective potential with Gaussian form factor*

We now try to simulate the above-mentioned characteristics of the complex effective N-N interaction by a linear combination of the Gaussian form factors as Eqs. (2·18) and

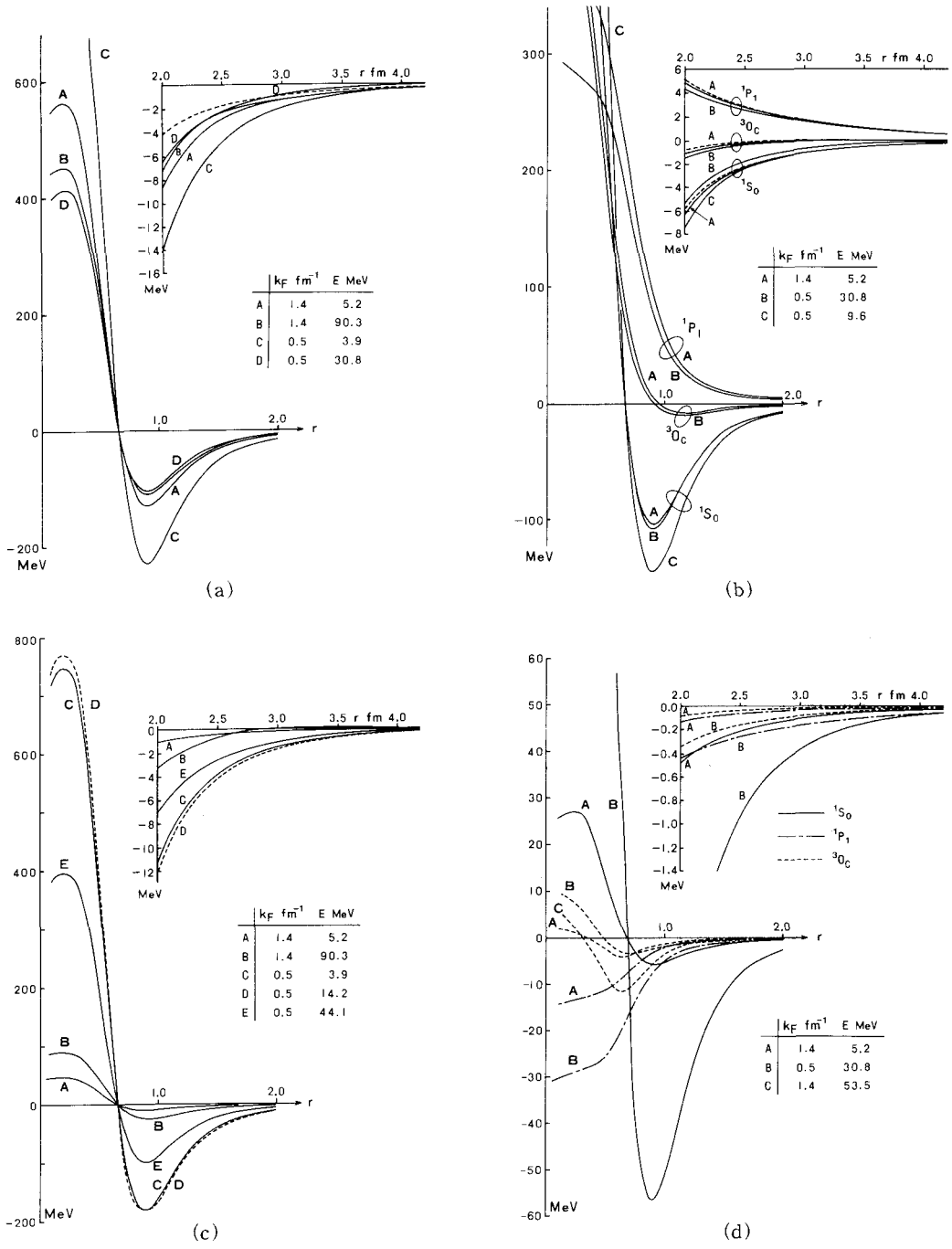

Fig. 5.(a) Some typical effective interactions $^{\text{eff}}t(r; k_F, E; \text{OPEG})$ which are numerically obtained with the use of Eq. (2·17). For the case of the real $^3S_1$ state. The dotted line denotes the central potential of OPEG.

(b) Same as (a). For the cases of the real $^1S_0$ and $^1P_1$ states and the triplet odd central component. The dotted lines denote the central potentials of OPEG.

(c) Same as (a). For the case of the imaginary $^3S_1$ state.

(d) Same as (a). For the cases of the imaginary $^1S_0$ and $^1P_1$ states and the triplet odd central component.

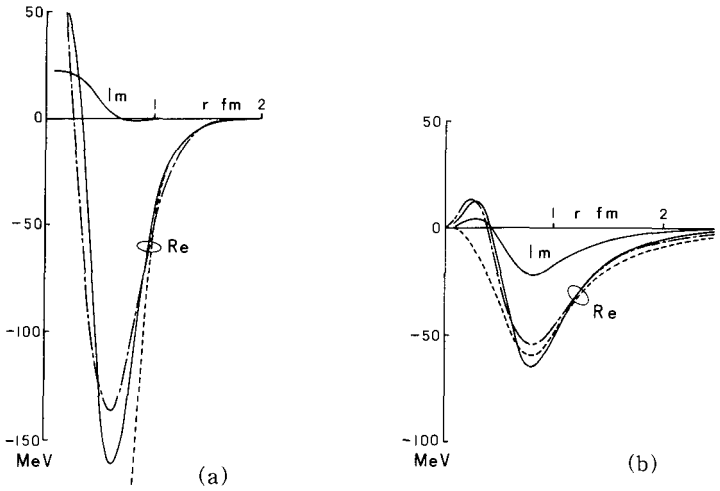

Fig. 6.(a) The spin-orbit component in the triplet odd state. The solid line denotes the numerical result at $k_F=1.1$ fm^{-1} and $E=48.6$ MeV with the use of Eq. (2·17). The dash-dotted line shows the functionalized potential, CEG in Table II. The basic OPEG is also shown by the dotted line.
(b) Same as (a). For the S-D tensor component in the triplet even state.

(2·19). It may not be satisfactory to use only three ranges of Gaussian form factors to obtain an overall fit to the radial dependence of the effective interaction. As we have discussed in § 3.a for the OMP, the derived effective interaction ${}^{\text{eff}}t(r; k_F, E)$ also depends on the basic nuclear force. The behavior of the tail of the effective interaction, however, is expected to be similar for HJ and OPEG in the sense that both of them originally have the OPEP tail. And so we first try to simulate the tail behavior and fit the second range region approximately and then adjust the core parameters so as to reproduce the bulk properties such as partial-wave-contributions to the BHF potential $U_\infty(E(k); k_F)$. This procedure corresponds to reproducing the diagonal matrix elements $\langle q|t|q\rangle$ in an average way.

In this paper we present a complex effective interaction whose parameters are adjusted to reproduce the results by HJ. In other words, we can say that this interaction is adjusted to reproduce approximately the results by OPEG including the ω-rearrangement effect, $(1-\bar{x})\cdot U_\infty(\text{OPEG})$. It seems that this parametrization is more favourable to reproducing the phenomenological OMP for finite nuclei in the density-dependent folding model as we will show in the following.

It being quite difficult to simulate the energy dependences of the obtained parameters by analytic functions, we tabulate the parameters in Eq. (2·19) for the energies $E=5$, 10, 20, 30 and 50 MeV in Table I together with the range parameters. The parameters for the non-central parts are shown in Table II. In this paper only the real parts of the non-central potentials are presented, because the imaginary parts are small and seem not to be important. We call this parametrized complex effective N-N interaction as CEG (Complex Effective potential with Gaussian form factor) hereafter.

We show to what extent this CEG can follow the numerical results of the OMP in nuclear matter. In Fig. 7 the calculated results of the partial-wave-contributions to the OMP using CEG are shown. In Figs. 6 and 8 the radial dependence of CEG is compared with that of the numerical results by OPEG for some components. In Fig. 8 we use the parameters for $E=50$ MeV in Table I. We can say from these figures that CEG follows

Table I. Parameters of the central polential of CEG.
Range parameters (fm); $\lambda_1=2.500$, $\lambda_2=0.8900$, $\lambda_3=0.5000$.

$E=5.0$ MeV

		Re			Im		
	i	v_0(MeV)	α(fm)	β(fm^2)	v_0(MeV)	α(fm)	β(fm^2)
	1	7.540	.0000	.0000	−.2434	−.3029	.1524
^1O	2	120.4	−.5583	.5062	−6.041	−.8586	.6442
	3	49.48	−.8833	1.614	−43.47	−1.055	.6318
	1	−5.034	−.3716	.1840	−11.86	−1.418	.5389
^3E	2	−829.4	−.6721	.2233	−1051.	−1.214	.3649
	3	1359.	−.2171	.1349	2406.	−1.031	.2386
	1	−3.928	.1839	−.1414	−2.282	−1.153	.4097
^1E	2	−490.9	−.3386	.1079	−245.8	−.9627	.2366
	3	1293.	−.03618	.01791	686.2	−.7508	.1161
	1	.6390	.0000	.0000	−.1776	−.9531	.2711
^3O	2	−109.7	.1447	−.2068	−2.065	7.153	−4.260
	3	349.1	1.144	−.3268	6.904	1.781	−1.073

$E=10.0$ MeV

		Re			Im		
	i	v_0(MeV)	α(fm)	β(fm^2)	v_0(MeV)	α(fm)	β(fm^2)
	1	7.540	.0000	.0000	−.2857	−.3029	.1524
^1O	2	120.4	−.5583	.5062	−6.686	−.8586	.6442
	3	49.48	−.8833	1.614	−50.78	−1.055	.6318
	1	−3.107	.3999	−.1013	−11.01	−1.309	.4711
^3E	2	−627.8	−.3469	.07080	−1044.	−1.226	.3831
	3	1238.	−.1061	.1003	2402.	−1.077	.2861
	1	−2.385	1.145	−.5047	−2.133	−1.052	.3533
^1E	2	−456.7	−.2614	.07866	−266.7	−1.024	.2827
	3	1221.	.007585	.01517	711.2	−.7912	.1471
	1	.6390	.0000	.0000	−.2209	−.7133	.1425
^3O	2	−109.7	.1447	−.2068	−1.883	9.204	−5.310
	3	349.1	1.144	−.3268	7.189	2.510	−1.592

$E=20.0$ MeV

		Re			Im		
	i	v_0(MeV)	α(fm)	β(fm^2)	v_0(MeV)	α(fm)	β(fm^2)
	1	7.540	.0000	.0000	−.3700	−.3029	.1524
^1O	2	120.4	−.5583	.5062	−7.974	−.8586	.6442
	3	49.48	−.8833	1.614	−64.71	−1.055	.6318
	1	−1.267	2.961	−.9211	−8.944	−1.112	.3478
^3E	2	−362.7	.5642	−.3421	−887.8	−1.150	.3504
	3	1025.	.1742	.003614	2316.	−1.129	.3479
	1	−1.364	2.234	−.6654	−1.890	−.8475	.2341
^1E	2	−403.0	−.1216	.02987	−298.2	−1.114	.3515
	3	1129.	.07923	.004921	730.7	−.8148	.1723
	1	.6390	.0000	.0000	−.2759	−.3356	−.06711
^3O	2	−109.7	.1447	−.2068	−3.039	6.042	−3.382
	3	349.1	1.144	−.3268	7.996	3.517	−2.304

(continued)

$E=30.0$ MeV

		Re			Im		
	i	v_0(MeV)	α(fm)	β(fm^2)	v_0(MeV)	α(fm)	β(fm^2)
	1	7.540	.0000	.0000	−.4537	−.3029	.1524
^1O	2	120.4	−.5583	.5062	−9.258	−.8586	.6442
	3	49.48	−.8833	1.614	−77.79	−1.055	.6318
	1	−.5459	8.287	−2.476	−7.040	−.9422	.2367
^3E	2	−295.2	.8759	−.4392	−655.8	−.9400	.2344
	3	893.5	.4013	−.07047	2148.	−1.137	.3777
	1	−1.281	1.777	−.2458	−1.704	−.6499	.1163
^1E	2	−370.5	−.03919	.007997	−300.8	−1.115	.3595
	3	1081.	.1038	.01028	743.0	−.8295	.1894
	1	.6390	.0000	.0000	−.2952	.1405	−.3513
^3O	2	−109.7	.1447	−.2068	−4.656	3.783	−2.029
	3	349.1	1.144	−.3268	9.806	3.589	−2.408

$E=50.0$ MeV

		Re			Im		
	i	v_0(MeV)	α(fm)	β(fm^2)	v_0(MeV)	α(fm)	β(fm^2)
	1	7.540	.0000	.0000	−.6193	−.3029	.1524
^1O	2	120.4	−.5583	.5062	−11.82	−.8586	.6442
	3	49.48	−.8833	1.614	−101.7	−1.055	.6318
	1	−.3852	10.29	−2.260	−4.144	−.8874	.1877
^3E	2	−270.4	.7970	−.3287	−358.5	−.3306	−.1033
	3	720.7	.8222	−.2056	1582.	−.9831	.3185
	1	−1.089	2.168	−.2551	−1.394	−.1992	−.1594
^1E	2	−321.2	.1251	−.04036	−248.6	−.9169	.2473
	3	1017.	.1639	.0000	748.7	−.8624	.2251
	1	.6390	.0000	.0000	−.3885	.4242	−.5243
^3O	2	−109.7	.1447	−.2068	−7.372	2.412	−1.281
	3	349.1	1.144	−.3268	14.73	3.037	−2.093

Table II. Parameters of the non-central potentials of CEG.

Spin-orbit potential in ^3O state

i	λ_i(fm)	v_0(MeV)
1	0.6742	−518.8
2	0.4394	637.0

Tensor potential in ^3E state

i	λ_i(fm)	v_0(MeV·fm^{-2})
1	1.374	−12.42
2	0.7217	−271.2
3	0.3343	830.9

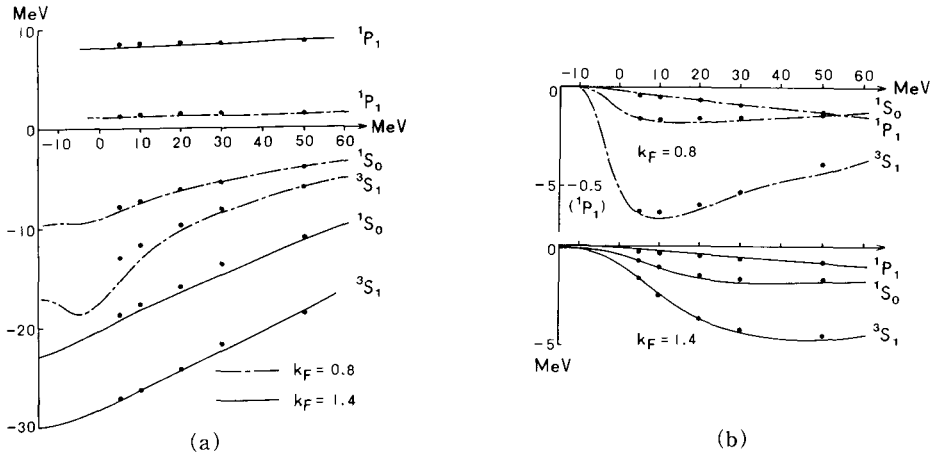

Fig. 7.(a) Comparision of some partial wave contributions to the real OMP $V_\infty(E(k); k_F)$ at $k_F=0.8$ and 1.4 fm^{-1}. The calculated results with CEG are denoted by black circles.
(b) Same as (a). For the imaginary OMP $W_\infty(E(k); k_F)$.

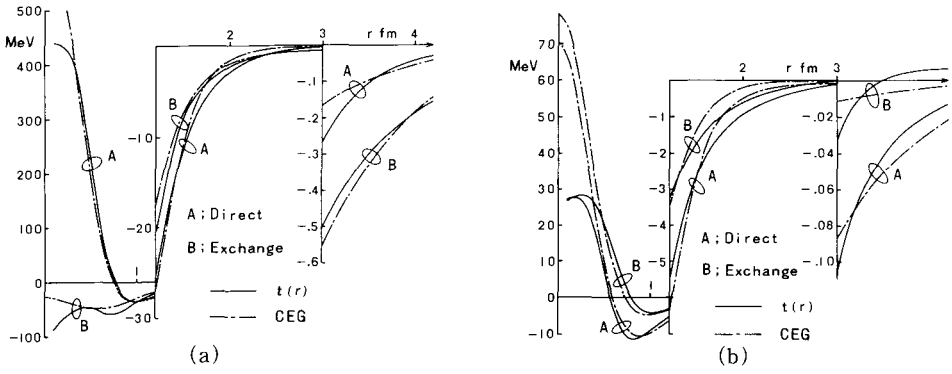

Fig. 8.(a) Radial behavior of the real part of the effective interaction $T_{D.EX}(r; k_F=1.4 \text{ fm}^{-1}, E=53.5$ MeV). The solid line is the numerical result from OPEG. The result of CEG is calculated with the parameters for $E=50$ MeV in Table I.
(b) Same as (a). For the imaginary part.

the overall behavior of the nuclear matter results quite well in these k_F and E.

3.b.3. *Application to finite nuclei in the folding model*

We calculate, using CEG, the folding potential, the differential cross sections and polarizations for $p+^{40}$Ca elastic scattering. The density distribution of ^{40}Ca is taken from Ref. 25). In Fig. 9 the folding potentials for various energies are shown, where the imaginary part is obtained by Eq. (2·24) using m_k/m given in Ref. 4). It is clearly seen that the imaginary part changes from the surface to volume type as the energy increases. Using these potentials, we calculate the differential cross sections and polarizations for the incident energies $E=21.0$, 30.3 and 48.0 MeV. The results are shown in Figs. 10(a) and (b) together with those by the conventional Woods-Saxon potential. Only with a renormalization factor N_I for the strength of the imaginary part the experimental results are nicely reproduced for these three energies. As for the spin-orbit part, we use the same spin-orbit potential as that of the phenomenological ones in order to compare our central

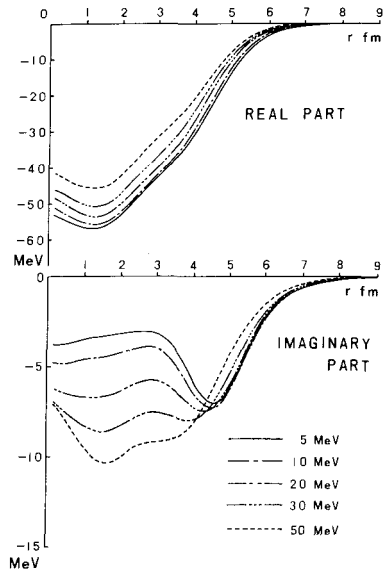

Fig. 9. Energy dependence of the folding potential obtained using CEG for the $p+^{40}$Ca scattering. The imaginary part is calculated with the use of Eq. (2·24).

CEG and its energy dependence with those of the Woods-Saxon potential. One case with the spin-orbit part of CEG is shown for $E=48.0$ MeV in Figs. 10(a) and (b). The result is satisfactory without renormalization. For other energies similar results are obtained. Here we do not try to search for the χ^2-minimum. Comparison of the potentials is shown in Fig. 11 in the two cases. It is said that our folding potential by CEG well follows the phenomenological one, but the volume integral J_R and the rms radius $\sqrt{\langle r^2\rangle}$ of the real potential do not necessarily agree with those obtained by the phenomenologically best-fit potential as seen in Table III.

§ 4. Summary

We have calculated the transition matrix and the optical potential in the LOBT self-consistently in the nuclear matter with the use of the basic nuclear forces OPEG and HJ. The following are found and concluded:

(1) The resultant optical potentials are strongly dependent on the basic nuclear forces. The stronger core singularity and $v_T/v_C(^3E)$ ratio lead to the weaker optical model potential. The OMP depth from HJ is weaker by about 10 MeV near the normal density than that from OPEG and that from RHC will be still weaker. This situation is analogous to that in the binding energy calculation.

(2) The ω-rearrangement potential adds an appreciably repulsive effect at higher densities. For example, it amounts to about 10 MeV for OPEG at $k_F \sim 1.4$ fm^{-1}. If we take into account the Pauli-rearrangement diagram, it will further weaken the OMP.[31]

(3) The anomaly in the real part of OMP arises just above the Fermi momentum and comes almost entirely from the $^3S_1+^3D_1$ partial wave contribution. The origin of this anomaly lies in the revival of the Pauli excluded space and also in the strong tensor coupling effect. In other words, this reflect the fact that an incident nucleon has a tendency to form a quasi-deuteron state with nucleons in the target at very low relative momenta. The enhancement of the anomaly in lower densities is readily understood from the above consideration.

(4) The coordinate represented transition matrix is calculated and simulated with three-range Gaussian form factor (we name it CEG). The transition matrix in the tail region is compared with OPEP and found to be strongly dependent on the density and energy in the ^3E state. The k_F- and E-dependences are retained in CEG and the strength is adjusted to reproduce the partial wave contributions to the optical potential by the HJ force. This is also understood to be the one adjusted to the result by OPEG renormalized with the ω-rearrangement.

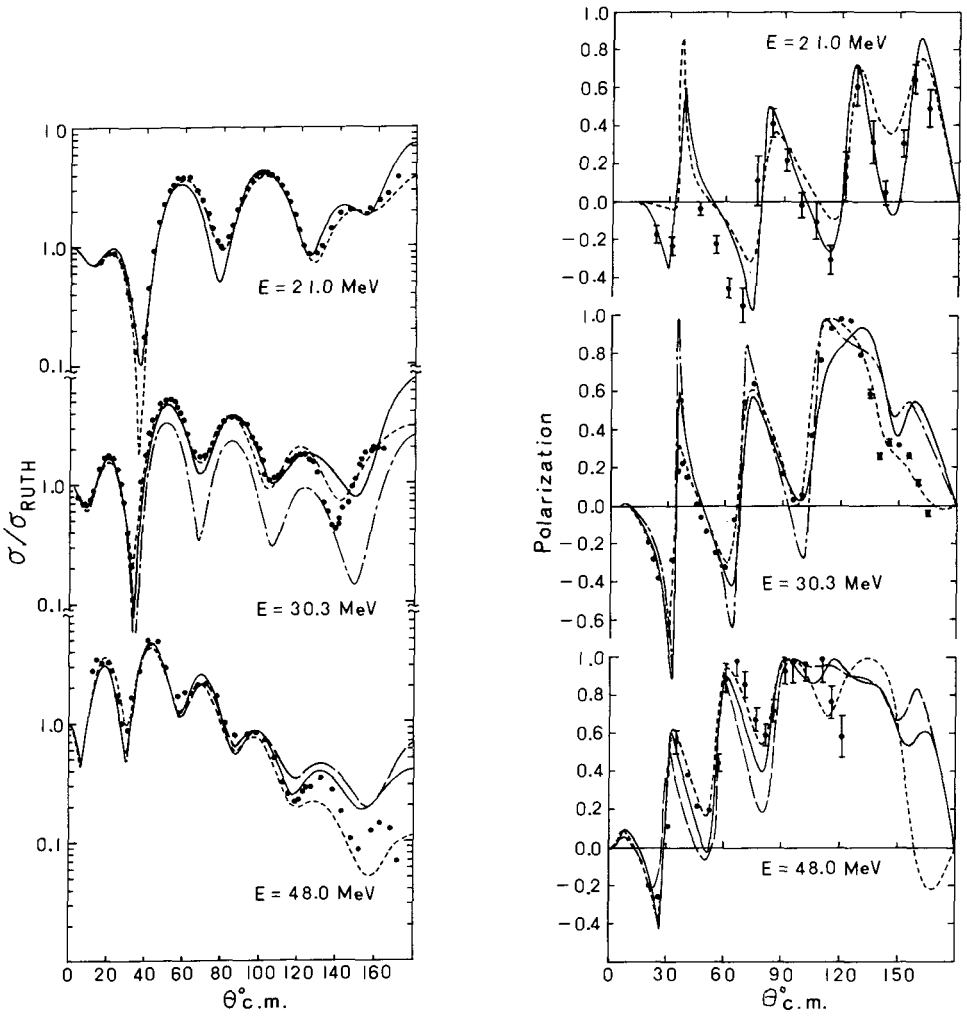

Fig. 10.(a) Differential cross section divided by the Rutherford cross section for the elastic scattering of proton from ^{40}Ca. The dotted lines represent the conventional OMP fits.[26),27)] The solid lines are calculated from the folding potentials using CEG with $N_I=0.7$, 0.7 and 0.8 for $E=21.0$, 30.3 and 48.0 MeV, respectively. The spin-orbit potentials are the same as those of optical model fits. The dash-dotted line in the case $E=30.3$ MeV is the same as the solid line except $N_I=1.0$. The dashed line in the case $E=48.0$ MeV is the same as the solid line except that the spin-orbit potential is of CEG. The experimental data are of Refs. 26) and 28).

(b) Polarizations for the elastic scattering of proton from ^{40}Ca. The experimental data are of Refs. 26), 29) and 30). The lines are the same as those in (a).

Table III. Calculated volume integrals J_R and rms radii of the real parts of conventional OMP and folding potentials from the $^{\text{eff}}t(r)$(OPEG) and CEG, at $E=30.3$ MeV in the case of $p+^{40}$Ca.

	J_R(MeV·fm^3)	$\sqrt{\langle r^2\rangle}$(fm)
conventional OMP[30)]	−428.0	4.18
folding pot. from $t(r)$(OPEG)	−456.1	3.95
folding pot. from CEG	−395.1	3.85

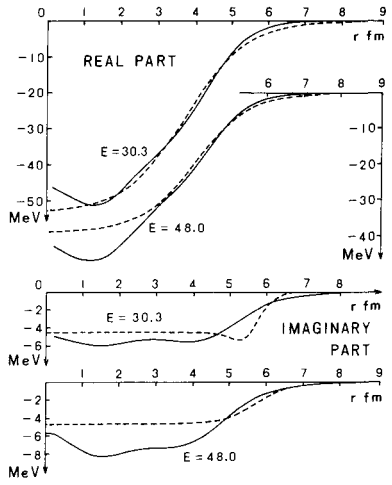

Fig. 11. Comparison of the folding potential with phenomenological potentials (dashed line).[26),27)]

(5) The differential cross sections and polarizations for the $p+^{40}$Ca elastic scattering are calculated with the folding potential obtained from CEG. The agreement with the experimental data are quite good for a wide region of the energy. The renormalization factor $N_I=0.7\sim0.8$ is necessary only for the imaginary part. The continum level density near the Fermi momentum employed in the nuclear matter calculation seems to be responsible for this overestimation of the imaginary part.

Here we comment on the relationship between the present "nuclear matter approach" and another microscopic approach which is called "nuclear structure approach". In the latter approach[5)] a matter of concern is a direct evaluation of the imaginary potential for finite nuclei, where the low excited collective states are explicitly taken into account and the imaginary potential of surface type is obtained. In our nuclear matter approach the particle-hole correlation diagrams are not included. On the other hand, in the structure approach the ladder term is assumed as real and the used effective interactions are not consistent with the Brueckner-Hartree-Fock term. Hence, we may say that these two approaches are, in the present stage, complementary to each other.

Finally, the present status of the microscopic calculation of the optical model potential based on the realistic nuclear force seems to correspond to the historical one step of the development in the binding energy problem. The LOBT clarifies some fundamental properties of the OMP in nuclear matter, but the experience in the binding energy problem suggests that the quantitative results may change depending not only on the nuclear force but also on the higher order corrections; for example, the off-energy-shell effect on the particle state energy, the rearrangement correction and three- and four-body cluster terms. On the other hand, the overestimation of the theoretical imaginary part is a new problem. It may be possible to reduce it, if we take the off-energy-shell effect and the QTQ spectra together with a resummation of diagrams in the hole-line expansion.

Acknowledgements

The authors are greatly indebted to Professor T. Sakuda and Professor H. Bando for continuous discussions and valuable comments and also for reading of the manuscript. They would like to thank Dr. H. Sakaguchi for fruitful suggestions based on his experimental results. They also would like to thank Mr. Y. Sakuragi for calculations to check the complex effective interaction and to thank Mr. T. Kasuga for drawing of the figures. One of the authors (N.Y.) is thankful to the colleagues in Nuclear Physics Laboratory in Oxford University for their kind hospitality and discussion on caluclation of OMP.

This work was partly supported by the annual research project (1982) on "Nuclear Molecular-like Structure and Light-Heavy-Ion Reaction" organized by the Research

Institute for Fundamental Physics. The numerical computations were carried out at the Computer Centers of Kyushu and Miyazaki Universities.

References

1) H. Sakaguchi et al., Phys. Lett. **89B** (1979), 40.
H. Sakaguchi et al., Phys. Lett. **99B** (1981), 92.
H. Sakaguchi et al., Phys. Rev. **C26** (1982), 944.
2) K. M. Watson, Phys. Rev. **89** (1953), 575.
K. A. Brueckner, R. J. Eden and N. C. Francis, Phys. Rev. **100** (1955), 891.
G. L. Shaw, Ann. of Phys. 8 (1959), 509.
A. K. Kerman, H. McManus and R. M. Thaler, Ann. of Phys. 8 (1959), 551.
J. S. Bell and E. J. Squires, Phys. Rev. Lett. **3** (1959), 96.
N. Vinh Mau, *Theory of Nuclear Structure*, Trieste Lectures, 1969 (IAEA, Vienna, 1970), p. 931.
J. Hufner and C. Mahaux, Ann. of Phys. **73** (1972), 525.
3) F. A. Brieva and J. R. Rook, Nucl. Phys. **A291** (1977), 299, 317; **A297** (1978), 206; **A307** (1978), 493.
4) J. P. Jeukenne, A. Lejeune and C. Mahaux, Phys. Rev. **C10** (1974), 1391; **C16** (1977), 80; Phys. Rep. **C25** (1976), 83.
5) N. Vinh Mau and A. Bouyssy, Nucl. Phys. **A257** (1976), 189.
A. Bouyssy, H. Ngo and N. Vinh Mau, Nucl. Phys. **A371** (1981), 173.
6) R. Sartor, Nucl. Phys. **A267** (1976), 29.
7) R. V. Reid, Ann. of Phys. **50** (1968), 411.
8) T. Hamada and I. D. Johnston, Nucl. Phys. **34** (1962), 382.
9) H. A. Bethe, B. H. Brandow and A. G. Petschek, Phys. Rev. **129** (1963), 225.
10) H. S. Köhler, Phys. Rep. **C18** (1975), 218.
B. D. Day, Rev. Mod. Phys. **50** (1978), 495.
11) G. Bertsch, J. Borysowicz, H. McManus and W. G. Love, Nucl. Phys. **A284** (1977), 399.
12) W. G. Love and F. Petrovich, *The (p, n) Reaction and the Nucleon-Nucleon Force*, edited by C.D. Goodman et al. (Plenum, New York, 1980).
W. G. Love, Phys. Rev. **C24** (1981), 1073.
13) G. R. Satchler, in Lecture Notes in Phys. **168** (Springer Verlag, 1982), p. 25.
W. G. Love, Phys. Rev. **C17** (1978), 1876.
G. R. Satchler and W. G. Love, Phys. Rep. **C55** (1979), 183.
A. M. Kobos, S. A. Brown, P. E. Hodgson, G. R. Satchler and A. Budzanowski, Nucl. Phys. **A384** (1982), 65.
14) B. H. Brandow, Rev. Mod. Phys. **39** (1967), 771.
Y. Akaishi, H. Bando, A. Kuriyama and S. Nagata, Prog. Theor. Phys. **40** (1968), 288.
15) P. J. Siemens, Nucl. Phys. **A141** (1970), 225.
16) Y. Akaishi and S. Nagata, Prog. Theor. Phys. Suppl. Extra No. (1968), 476.
17) K. A. Brueckner and J. L. Gammel, Phys. Rev. **109** (1958), 1023.
18) D. M. Brink and G. R. Satchler, *Angular Momentum* (Oxford Univ. Press, Oxford, 1968).
19) J. W. Negele and D. M. Vautherin, Phys. Rev. **C5** (1972), 1472.
20) J. W. Negele and K. Yazaki, Phys. Rev. Lett. **47** (1981), 71.
S. Fantoni, B. L. Friman and V. R. Pandharipande, Phys. Lett. **104B** (1981), 89.
21) R. Tamagaki, Prog. Theor. Phys. **39** (1968), 91.
22) N. Yamaguchi, T. Kasahara, S. Nagata and Y. Akaishi, Prog. Theor. Phys. **62**(1979), 1018.
23) I. Ahmad and M. Z. Rahman Khan, Nucl. Phys. **A144** (1970), 7.
V. Bernard and C. Mahaux, Phys. Rev. **C23** (1981), 888.
C. Mahaux and H. Ngo, Nucl. Phys. **A378** (1982), 205.
24) W. Haider, A. M. Kobos and J. R. Rook, private communication.
25) J. W. Negele, Phys. Rev. **C1** (1970), 1260.
26) K. H. Bray et al., Nucl. Phys. **A167** (1971), 57.
27) R. S. Mackintosh and L. A. Cordero-L, Phys. Lett. **68B** (1977), 213.
28) B. W. Ridley and J. F. Turner, Nucl. Phys. **58** (1964), 497.
29) V. Hnizdo et al., Phys. Rev. **C3** (1971), 1560.
30) R. M. Craig et al., Nucl. Phys. **86** (1966), 113.
31) M. Kohno and D. W. L. Sprung, Nucl. Phys. **A397** (1983), 1.